· Article · Advances in Polar Science

doi: 10.3724/SP.J.1085.2011.00101 June 2011 Vol.22 No.2: 101–110

Heat-induced temperature enhancement in the polar summer ionosphere

XU Bin[1*], CHENG MuSong[2], XU ZhengWen[1], WU Jun[1], WANG ZhanGe[1], XUE Kun[1] & WU Jian[1]

[1] National Key Laboratory of Electromagnetic Environment, China Research Institute of Radiowave Propagation, Qingdao 266107, China;
[2] School of Science, Xidian University, Xi'an 710071, China

Received April 6, 2011; accepted May 27, 2011

Abstract Observation data recorded by the European Incoherent Scatter Scientific Association in Tromsø, Norway in August 2009 were analyzed to determine the heating effects in polar summer ionospheric modification experiments. There are two types of increases in electron temperature: large relative increases in a narrow range near 150 km and greater absolute increases in a wider range at 150–400 km. The percentage increase in temperature linearly increases with heating power, but the rate of increase decreases with increasing pump frequency. A clear two-dimensional distribution was found for the measurement made on August 15, and the heating effects are greater closer to the direction of the geomagnetic field. The heating effects obviously depend on the angle between the heating beam and geomagnetic field; as the angle increases, the heating effect decreases.

Keywords **Ionosphere heating, European Incoherent Scatter Scientific Association, electron temperature enhancement, polar ionosphere**

Citation: Xu B, Cheng M S, Xu Z W, et al. Heat-induced temperature enhancement in the polar summer ionosphere. Adv Polar Sci, 2011, 22: 101—110, doi: 10.3724/SP.J.1085.2011.00101

0 Introduction

In an active space-plasma experiment, plasma parameters are controlled artificially to better clarify turbulence, discharge and nonlinear processes and wave-wave and wave-particle interactions. Thus, active experiments are important in space science. With the injection of high-power radiowaves into the ionosphere, there is nonlinear interaction between waves and particles, which enhances ion and plasma lines and SEE (Stimulated Electromagnetic Emission)[1–3], airglow[4–5], excitation of very-low frequency, extremely-low frequency and ultralow-frequency waves[6] and Langmuir turbulence[7]. It is also important to investigate the increase in electron temperature as an indicator of the absorption rate of high-frequency (HF) pump waves. Temperature increases induced by HF pump waves have been widely discussed since they were first reported by Gordon[8–9]. Nighttime observations of electron heating at Arecibo indicated temperature increases of some 40% (about 350 K)[10]. A much larger increase of about 1000 K – 2000 K was recorded in an experiment carried out at night in winter at the solar minimum, and the difference is explained by the much lower cooling rate resulting from lower density[11]. In high-latitude regions, most measurements have been made during the day when the ionosphere is more stable[12–14], and the electron temperature has been found to increases about 55%. However, a greater increase of up to 300% was observed in a nighttime experiment[15]. It is difficult to determine ionospheric parameters accurately in a low-altitude ionosphere region owing to large measurement error and low spectral resolution, but the temperature phenomenon has still been observed in such regions[16–17]. In addition, the oscillation in electron temperature induced by heating[18] and temperature isotropy in the E region[19–20] have also been investigated.

This paper presents heating-induced features of the polar summer ionosphere in 2009. The heating and diagnosis

* Corresponding author(email: jasur1982@sina.com)

facility and the experiment setting are first described and the effect of the temperature increase, two different heating cases and the two-dimensional (2D) aspect sensitivity are then discussed.

1 Experiment overview

The heating campaign was carried out in Norway during August 13–15, 2009. The European Incoherent Scatter Scientific Association (EISCAT) heating facility is located in Tromsø (69.59 °N, 19.23 °E), northern Norway, and has three heating arrays. In light of the low ionospheric critical frequency, antenna array 2 was used in this experiment to satisfy the over-dense heating condition. The pump frequencies vary within the range 4.04–4.912 8 MHz depending on the local ionosphere state. The pump beam was pointed such that it was field-aligned on August 13–14, and the beam was operated in scanning mode on August 15. The heating schedule is detailed in Figure 1 (in universal time, UT). The main diagnosis instrument is the ultra-high frequency (UHF) incoherent-scatter radar, which we operated in experiment mode Beata. In the heating experiment conducted on August 15, the scanning mode was revised to match the pump beam. The scan Sector adjusts automatically with a change in pump beam as shown in Figure 2, where a solid line is the direction of the UHF beam and the bold dashed line is the direction of the heating beam.

Heating schedule for August 13, 2009											
8:16	8:20	8:24	8:28	8:32	8:36	8:40	8:44	8:48	8:52	8:56	9:00
Circle 1：33%–66%–100% 4.04 MHz						Circle 2：33%–66%–100% 4.04 MHz					
9:04	9:08	9:12	9:16	9:20	9:24	9:28	9:32	9:36	9:40	9:44	9:48
Circle 3：33%–66%–100% 4.04 MHz						Circle 4：33%–66%–100% 4.04 MHz					
9:52	9:56	10:00	10:04	10:08	10:12	10:16	10:20	10:24	10:28	10:32	10:36
Circle 5：33%–66%–100% 4.04 MHz						Circle 6：33%–66%–100% 4.544 MHz					
10:40	10:44	10:48	10:52	10:56	11:00	11:04	11:08	11:12	11:16	11:20	11:24
Circle 7：33%–66%–100% 4.544 MHz						Circle 8：33%–66%–100% 4.04 MHz					
11:28	11:32	11:36	11:40	11:44	11:48	11:52	11:56	12:00	12:04	12:08	12:12
Circle 9：33%–66%–100% 4.04 MHz						Circle 10：33%–66%–100% 4.544 MHz					
12:16	12:20	12:24	12:28	12:32	12:36	12:40	12:44	12:48	12:52	12:56	13:00
Circle 11：33%–66%–100% 4.04 MHz						Circle 12：33%–66%–100% 4.04 MHz					
Heating schedule for August 14, 2009											
8:00	8:04	8:08	8:12	8:16	8:20	8:24	8:28	8:32	8:36	8:40	8:44
Circle 1：33%–66%–100% 4.04 MHz						Circle 2：33%–66%–100% 4.04 MHz					
8:48	8:52	8:56	9:00	9:04	9:08	9:12	9:16	9:20	9:24	9:28	9:32
Circle 3：33%–66%–100% 4.04 MHz						Circle 4：33%–66%–100% 4.544 MHz					
9:36	9:40	9:44	9:48	9:52	9:56	10:00	10:04	10:08	10:12	10:16	10:20
Circle 5：33%–66%–100% 4.544 MHz						Circle 6：33%–66%–100% 4.544 MHz					
10:24	10:28	10:32	10:36	10:40	10:44	10:48	10:52	10:56	11:00	11:04	11:08
Circle 7：33%–66%–100% 4.544 MHz						Circle 8：33%–66%–100% 4.544 MHz					
11:12	11:16	11:20	11:24	11:28	11:32	11:36	11:40	11:44	11:48	11:52	11:56
Circle 9：33%–66%–100% 4.04 MHz						Circle 10：33%–66%–100% 4.04 MHz					
12:00	12:04	12:08	12:12	12:16	12:20	12:24	12:28	12:32	12:36	12:40	12:44
Circle 11：33%–66%–100% 4.04 MHz						Circle 12：33%–66%–100% 4.04 MHz					
Heating schedule for August 15, 2009											
Circle 1	8:00		8:08		8:12		8:20		8:24		8:32
	12° 4.04 MHz				6° 4.04 MHz				0° 4.04 MHz		
Circle 2	8:36		8:44		8:48		8:56		9:00		9:08
	12° 4.04 MHz				6° 4.04 MHz				0° 4.04 MHz		
Circle 3	9:12		9:20		9:24		9:32		9:36		9:44
	12° 4.04 MHz				6° 4.04 MHz				0° 4.544 MHz		
Circle 4	9:48		9:56		10:00		10:08		10:12		10:20
	12° 4.544 MHz				6° 4.544 MHz				0° 4.544 MHz		
Circle 5	10:24		10:32		10:36		10:44		10:48		10:56
	12° 4.544 MHz				6° 4.544 MHz				0° 4.9128 MHz		
Circle 6	11:00		11:08		11:12		11:20		11:24		11:32
	12° 4.9128 MHz				6° 4.9128 MHz				0° 4.544 MHz		
Circle 7	11:36		11:44		11:48		11:56		12:00		12:08
	12° 4.544 MHz				6° 4.544 MHz				0° 4.544 MHz		

Figure 1 Schedule of the ionospheric heating experiment (grey: O-mode heating, white: no heating).

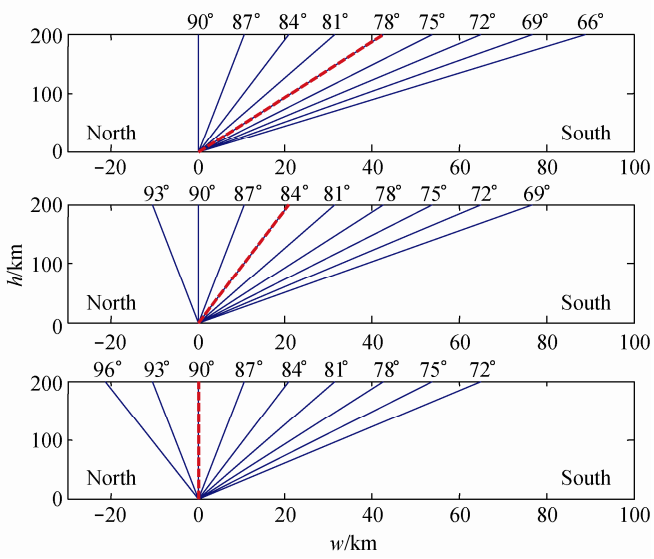

Figure 2 Scanning area of the UHF radar. A solid line is the UHF beam direction and the bold dashed line is the heating beam direction.

2 Field-aligned heating

The official data analysis procedure GUISDAP (Grand Unified Incoherent Scatter Design and Analysis Package) was provided by EISCAT for normal data processing. The data analysis results with an integral time of 4 min are shown in Figure 3 for field-aligned ionospheric heating on August 13–14. There are large increases in electron

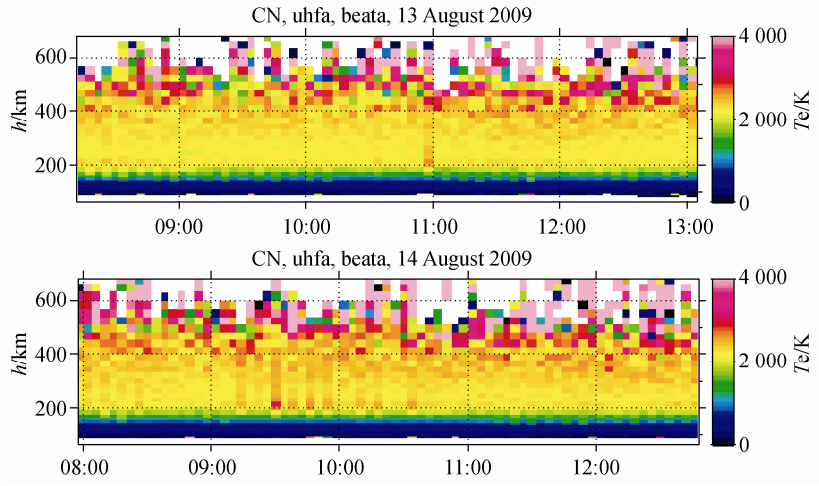

Figure 3 Increase in electron temperature from August 13 to 14, 2009.

temperature at 0816–1012 UT, 1056–1148 UT and 1224–1236 UT on August 13 between 150 and 200 km, but there is a wide range of temperatures from 150 to 400 km at 1056 UT. Analogously, there are temperature increases in a narrow height range at 0800–0828 UT, 0856–0908 UT and 1120–1244 UT on August 14. However, there are more cases of temperature increases on August 14. There is a clear wide range of temperature increases at 0912–1020 UT, except when heating at 33% power at 0936 UT and 1000 UT.

To further analyze the relationship between the temperature increases and pump power, Figures 4 and 5 present the electron temperature profile for varying power on August 13–14. A solid line is the average result for the three cases without heating, a long-dash line is the result for 33% pump power, a dotted line is the result for 66% pump power, and a short-dash line is the result for 100% pump power. The figures show that the electron temperature increases with an increase in pump power on August 13 except in cases 6, 10 and 12. The lack of an increase in cases 6 and 10 is due to the low pump frequency; the ionospheric critical frequency is lower than the working frequency of 4.544 MHz, and there is under-dense heating in these two cases. The lack of an increase in case 12 is due

to the change in the ambient ionosphere condition; the electron temperature increases at the non-heating time 1252 UT, and therefore, when the ionosphere plasma is heated with full power at 1256 UT, the heating effect is not as clear as that for 66% power at 1248 UT. The total heating effect on August 14 is greater than that on August 13, which is due to the higher critical frequency during the period 0800–1000 UT on August 14. This ensures that the over-dense heating condition is satisfied mostly with a pump frequency of 4.544 MHz. However, the dependence of the temperature increase on pump power on August 14 is not as strong as that on August 13. Because of under-dense heating, the heat-induced effect in case 8 is not obvious. Furthermore, pump-induced temperature increases are seen in cases 2, 5 and 7, but the amplitude of the temperature increase does not change monotonically with pump power.

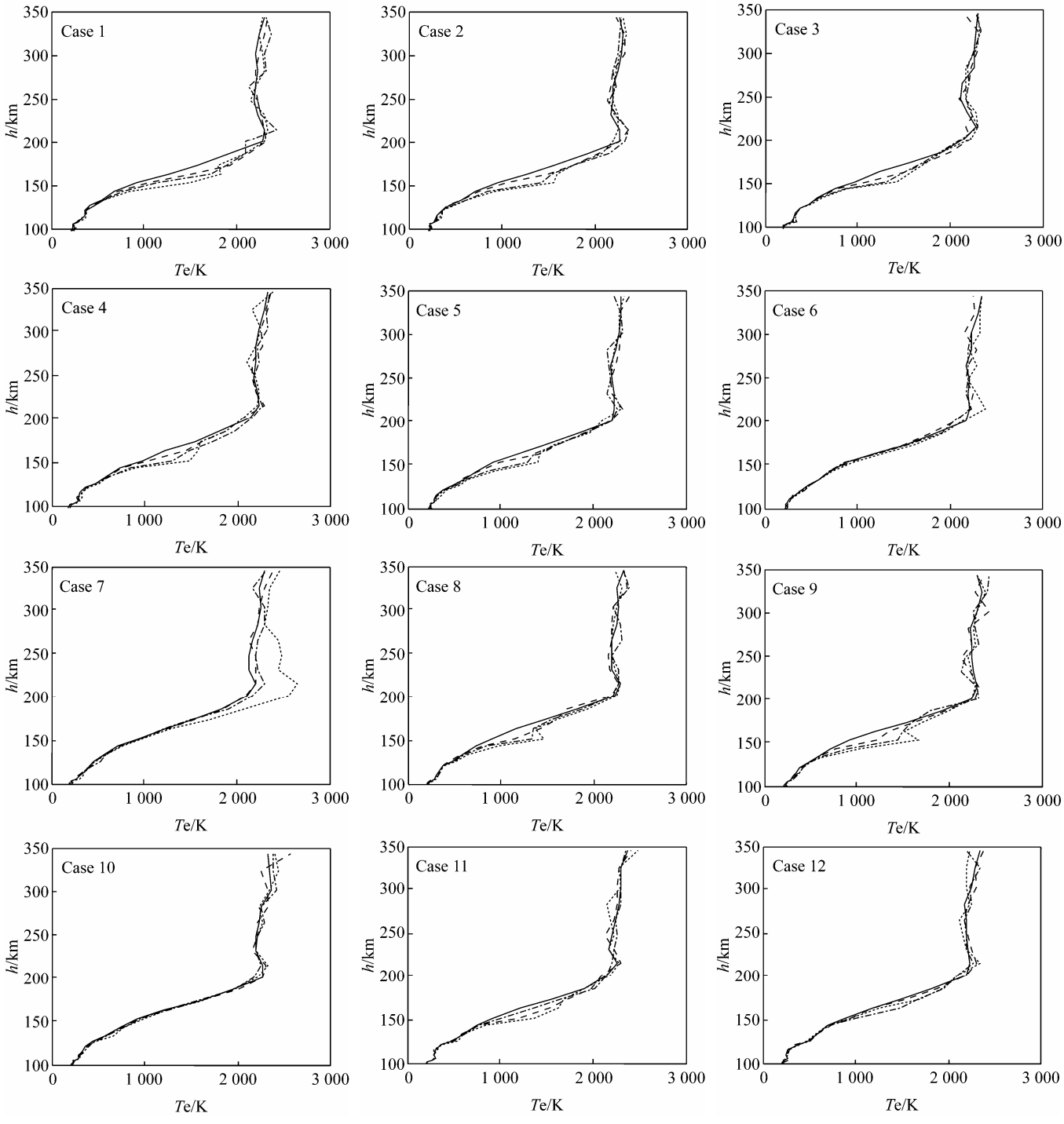

Figure 4 Electron temperature profiles during heating on August 13, 2009. The solid line is the result for no heating, the long-dash line is the result for 33% pump power, the dotted line is the result for 66% pump power, and the short-dash line is the result for 100% pump power.

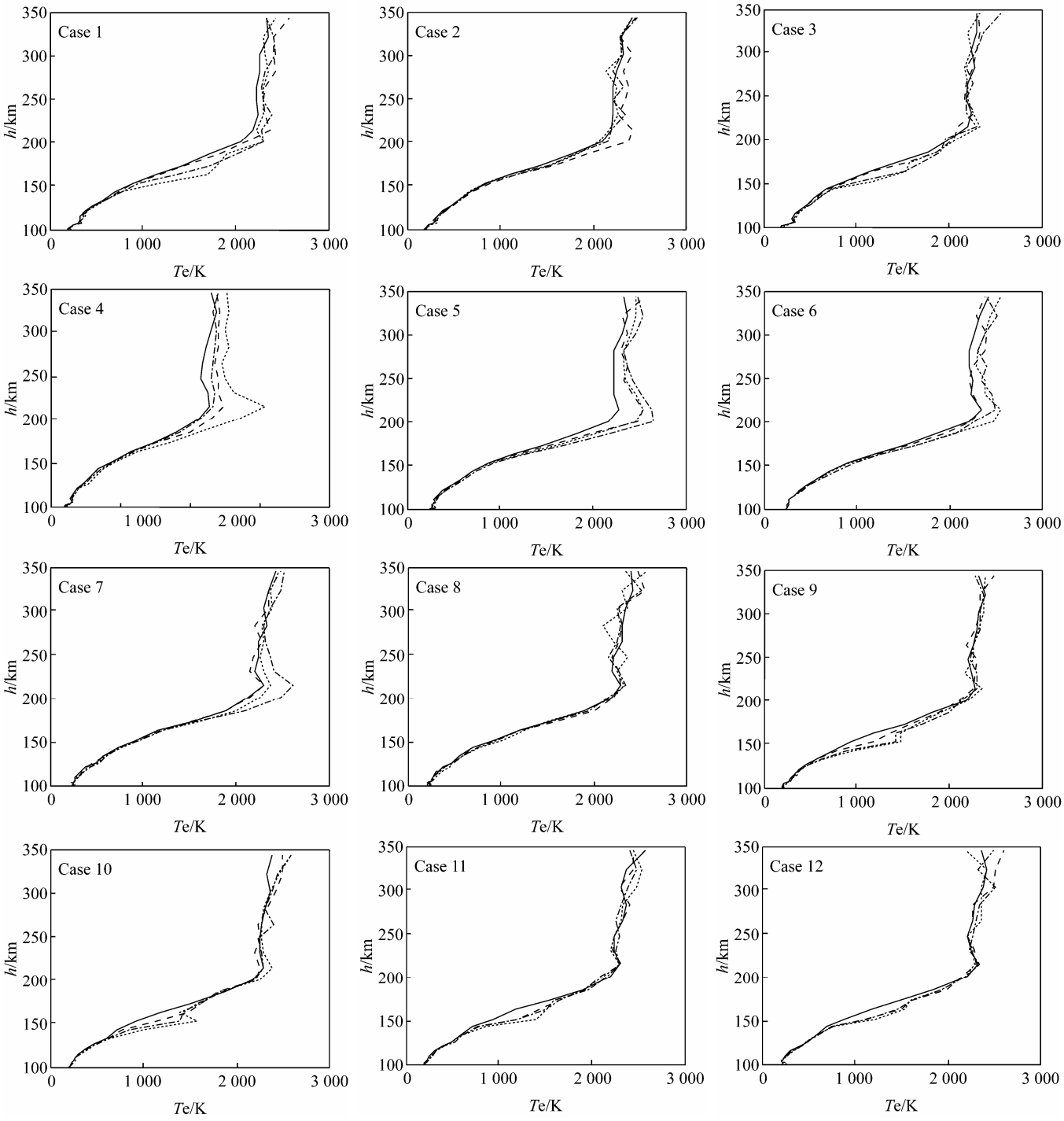

Figure 5 Electron temperature profiles during heating on August 14, 2009. The solid line is the result for no heating, the long-dash line is the result for 33% pump power, the dotted line is the result for 66% pump power, and the short-dash line is the result for 100% pump power.

As mentioned above, the temperature increases can be divided into two types: temperature increases in a narrow height range of 150–200 km, which have a clear peak, and temperature increases in a wide height range of 150–400 km, which are smooth. For the first type on August 13, the greatest increase is in case 9 at 1128–1152 UT, with the temperature increasing 35.07%, 54.22% and 81.58% with 33%, 66% and 100% pump power respectively. However, the timing of the smallest increase differs for the three power levels. The smallest increase for 33% pump power is in case 11 (1216 UT), with a percentage increase of 10.01%, that for 66% pump power is in case 1 (0824 UT), with a percentage increase of 29.31%, and that for full pump power is in case 3 (0920 UT), with a percentage increase of 41.28%. Similar to the results obtained for August 14, the maximum temperature increase for 33% and 66% power levels is in

case 9 (1112 UT, 1120 UT), with a percentage increase of 27.37% and 54.31%, and that for full power is in case 10 (11152 UT), with a percentage increase of 71.06%.

The minimum increases in temperature are in case 1 (0800 UT, 0808 UT) for 33% and 66% power levels, with percentage increases of 13.59% and 21.68%, and case 12 for full-power heating, with a percentage increase of 43.97%. The height range of the temperature increases is much larger for type 2, but the peak of the temperature change is lower, such as in case 6, for which there is a broad temperature peak. The percentage increase in electron temperature of type 2 is much less than that of type 1, having a maximum of only 37.05%. The pump frequency for the wide-range increase in temperature is 4.544 MHz, while that for the narrow-range increase is 4.04 MHz, which is consistent with simulation results[21].

To determine the quantitative relationship between the heating effect and pump power, regression analysis was carried out for the two heating types. For type 1, the change in the percentage increase in temperature with pump power is given in Figure 6 for cases 1–5, 8–9 and 11 on August 13 and cases 1 and 10–12 on August 14. Here the solid line is the regression result and the stars are measurement data. The regression line is $dT = 0.53P + 4.07$. For type 2, the change in the percentage increase in temperature with power is given in Figure 7 for case 7 on August 13 and cases 4–6 on August 14. The regression line is $dT = 0.15P + 5.60$. The slope for 4.04 MHz heating is 3.59 times that for 4.544 MHz heating.

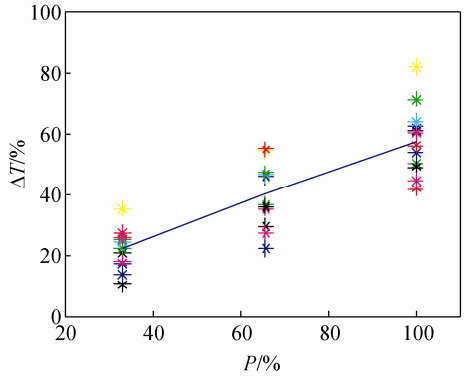

Figure 6 Regression analysis of the narrow-range temperature increase.

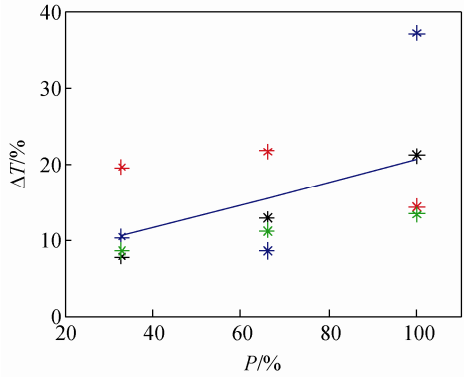

Figure 7 Regression analysis of the wide-range temperature increase.

3 2D scanning heating

A 2D scan of the heating region was carried out on August 15. The heating schedule and antenna scan mode are given in Figures 1 and 2. The UHF incoherent radar scanned about a center of 77.4° from 0800 UT for periods of 12 min. The UHF radar beam can be oriented from 0° to 90°, and by rotating the azimuth through 180°, from 90° to 180°. Although tests have confirmed that the radar can operate at elevations up to 96°, which would be satisfactory in this experiment, the radar azimuth rotates through 180° as the radar beam passes through the zenith, and measurement data are lost at these times. Analysis results from GUISDAP are shown in Figure 8.

There is a temperature increase around 150 km from 0800 UT to 0900 UT (case 1, case 2 and the first two sub-circles of case 3). After 0936 UT, the critical frequency of the ionosphere increased, and the pump frequency was increased to 4.544 and 4.912 8 MHz. Therefore, the temperature increase is larger in the experiment, such as at 0948 UT in case 4, 1024 UT in case 5, 1100 UT in case 6 and 1136–1156 UT in case 7. When the HF beam is field-aligned, there is direction dependence in the UHF Sector from 66° to 90° in all heating cases except case 6, and the best observations are made in cases 4 and 7. In cases 2 and 3, the temperature increase in the direction of 75° is close to the value for the field-aligned beam, but the latter is little larger. Increasing the deviation from

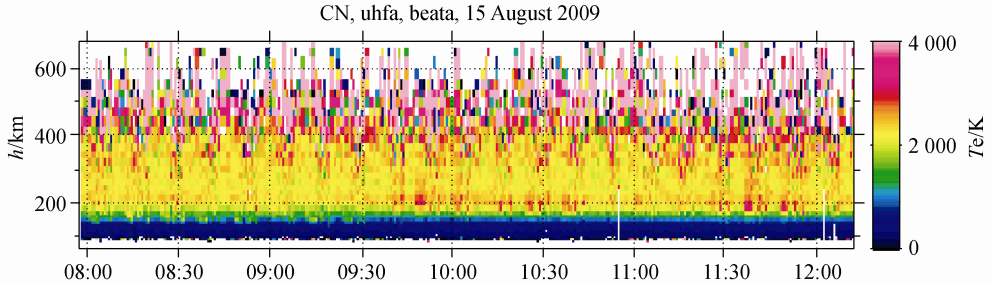

Figure 8 UHF heating effects on August 15, 2009.

field-aligned heating reduces the temperature increase. The increase in temperature is unclear in the directions of 66° and 90°, and the temperature sometimes returns to that for the ambient ionosphere. When the pump beam is pointed 6° south, the UHF radar scans from 69° to 93°. In this case, the average increase in the electron temperature is less than that for field-aligned heating. There is obvious aspect dependence on both sides of the Sector in cases 1 and 7 and the maximum is for heating 6° to the south. This phenolmenon is also observed in case 3, but the amplitude for an elevation of 75° approaches that for field-aligned heating in the right Sector, and there is a sudden increase in the vertical direction in the left Sector. There is only aspect dependence in the right Sector in cases 1, 4 and 5. With vertical pointing of the heating beam, there is aspect dependence in cases 1 (right Sector), 2 and 3, but the change in temperature is not clear. There are no 2D heating features in any other case.

To determine 2D statistical characteristics, the mean value of the electron temperature for different beam directions is calculated for the two types of temperature increase. For type 1, the temperatures in cases 1–3 are averaged for the three heating-beam directions. For type 2, the temperatures in cases 4, 5 and 7 are averaged for field-aligned heating and heating 6° to the south and the temperatures in cases 3 and 4 are averaged for the vertical beam. The averages are taken to obtain more accurate results. The results are presented in Figures 9 and 10.

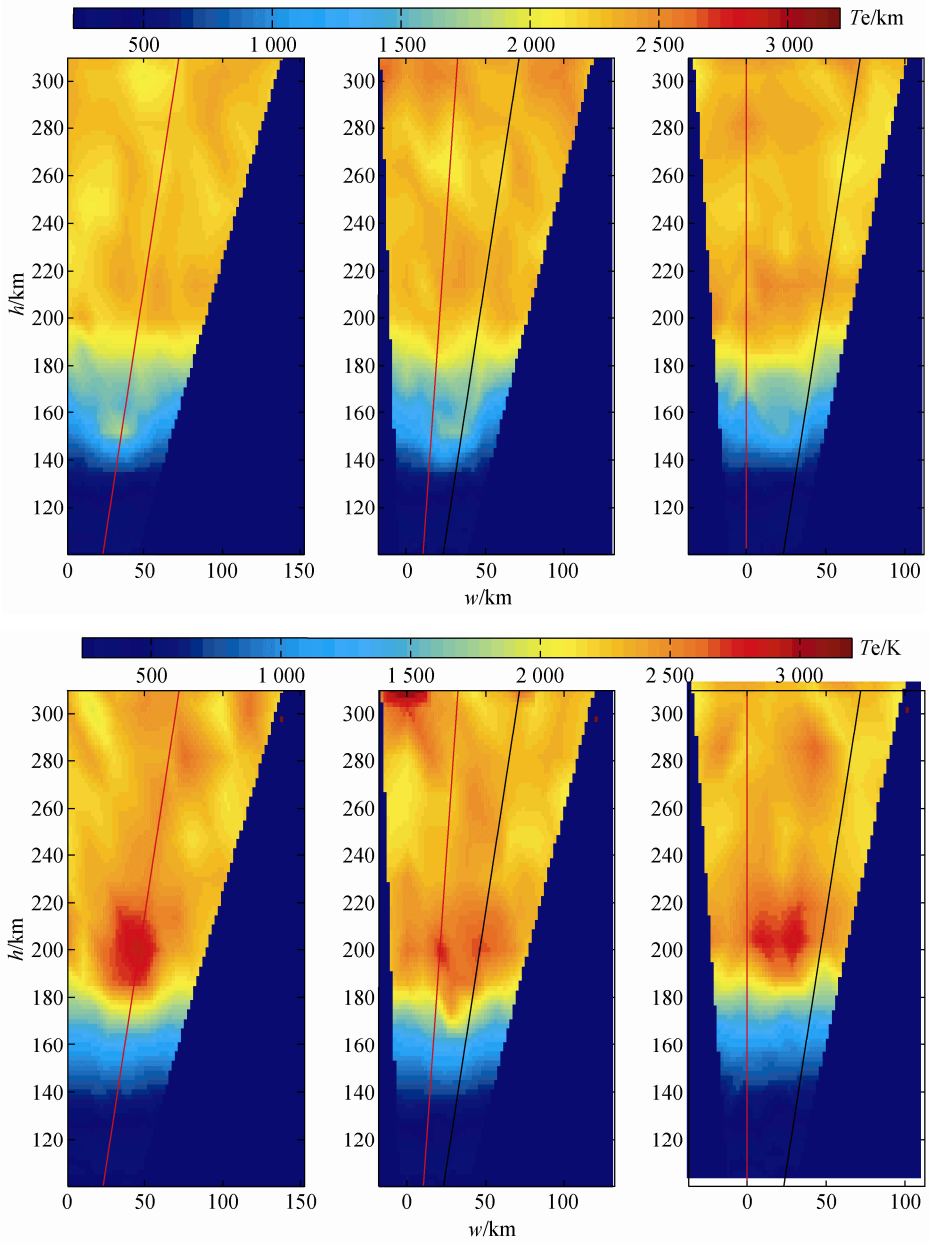

Figure 9 2D distribution of the electron temperature during heating on August 15, 2009 (top: type 1; bottom: type 2).

From left to right, the figures present data for field-aligned, 6° south and vertical heating directions. The directions of the heating beam and geomagnetic field are indicated by red and black lines respectively. The figures show that the best heating effect is at around 150 km for type 1 but 190 km for type 2. There is some commonality between the two types. The electron temperature maximum is in the direction of heating in the case of field-aligned heating, and between the directions of the geomagnetic field and the heating beam in the case of heating 6° to the south. With vertical heating, the phenomenon is the same as that for heating 6° to the south but the maximum is closer to the direction of the geomagnetic field.

Figure 10 presents the 2D distribution of the temperature increase. For type 1, the best heating effect is in the case of field-aligned heating, and the effect reduces quickly with increasing departure from field-aligned heating. That is, the peak of the heating effect is near the magnetic zenith[22]. Although the peak has a small offset to the north when the heating beam is directed northward, the change is not synchronous. For type 2, the distribution of the heating effect is similar to that for type 1 when the heating beam is vertical or field-aligned but not when it is 6° to the south, in which case there is a sudden increase in temperature. Figure 9 (bottom) shows that the spatial distribution of temperature when heating 6° to the south is anomalous, which differs from the case for vertical and field-aligned heating. When heating 6° to the south, there is a peak temperature increase at 300 km, but it cannot be attributed to heating during the experiment because the structure existed prior to heating. Although there is a lack of samples, only one abnormal case seriously affects the combined results. Thus, the heating

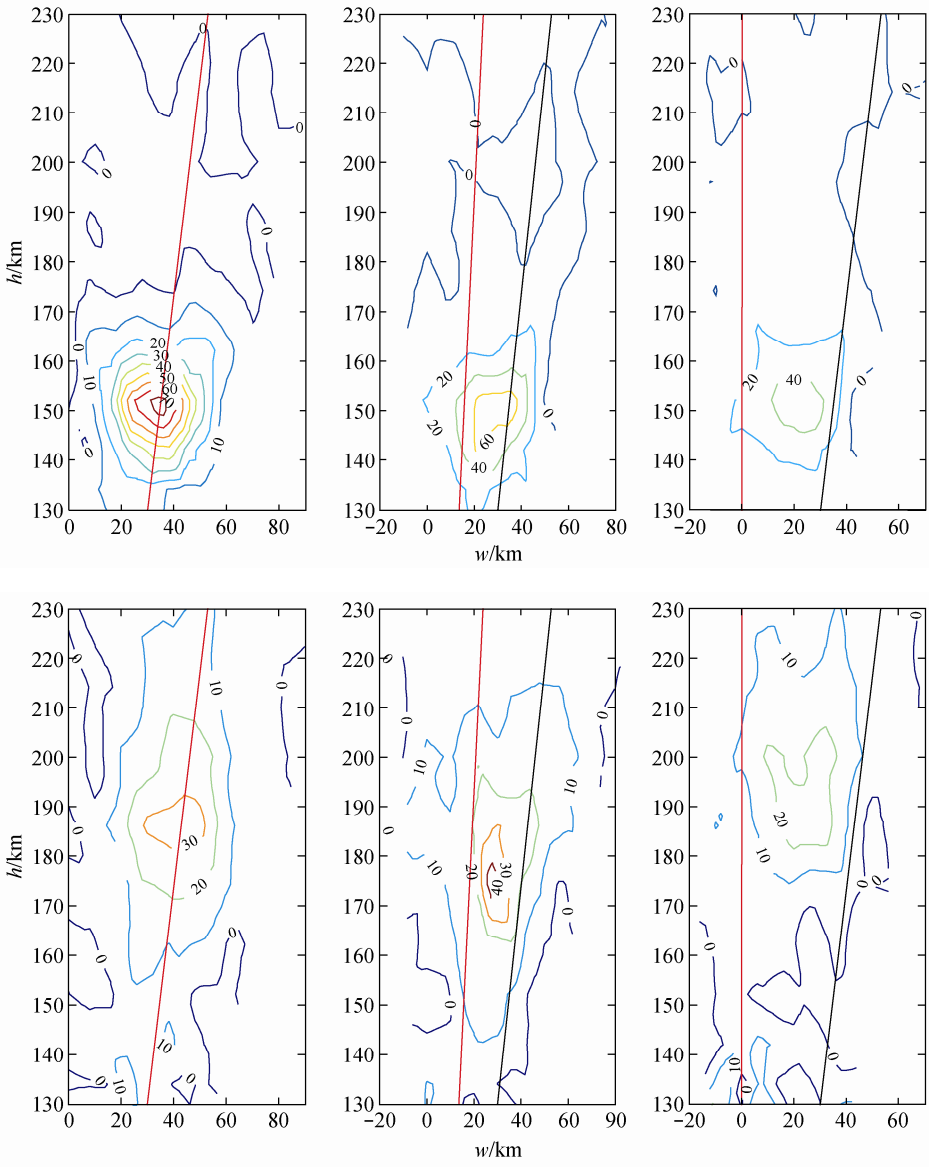

Figure 10 2D distribution of the electron temperature increase during heating (top: type 1; bottom: type 2).

abnormity for heating 6° to the south may be due to a change in the background ionosphere. In terms of the spatial distribution of the temperature increase, the heating on August 15 is similar to that on August 13–14. The type 1 increase has a symmetric Gaussian distribution in both landscape and longitudinal orientations. The type 2 increase is only symmetric in the landscape orientation, and the longitudinal scale is much larger than that for type 1. The temperature increase is asymmetric near the reflection height, with the increase in temperature being greater above the reflection height. This is because the neutral gas density increases with decreasing height below the reflection height, and the energy of the high-temperature electrons is easily lost in collisions. At greater height, there is rarefaction of neutral gas, and the HF heating energy is transported further. Overall, the angle between the heating beam and geomagnetic field plays an important role in energy absorption. Furthermore, owing to nonlinear interaction between high-power HF waves and ionospheric plasma, energy absorption does not cut off at the reflection height but extends far above.

4 Conclusions

A summer heating campaign was carried out during August 13–15, 2009 in Tromsø, Norway. In the over-dense heating case, in which the ionospheric critical frequency is higher than the pump frequency, there is a clear increase in the temperature of electrons. There are two aspects to theheating phenomena in this experiment: one is temperature increases in a narrow height range of 150–200 km, which have an obvious peak, and the other is temperature increases in a wider height range of 150–400 km, in which the maximum increase in temperature is obscure but the magnitudes of the temperature increases are larger. From regression analysis of the two types of increases, it is found that the relationship of the percentage increase in temperature with the pump power is linear, and the rate of the increase increases with decreasing pump frequency.

The aspect feature of the heating experiment was also investigated, and it is suggested that the heating effect has an obvious 2D distribution, with the maximum heating being close to the direction of the geomagnetic field. The temperature enhancement is centrosymmetric for type 1 temperature increases. For type 2 increases, the enhancement is symmetric in the landscape orientation, but the magnitude of the temperature increase in the direction of the geomagnetic field near the reflection height is asymmetric. The heating effect depends on the angle between the beam direction and the direction of the geomagnetic field evidently, with the heating effect weakening with increasing angle. In summary, this paper presented results for an ionospheric heating experiment and divided heating effects into two types. Different heating cases were discussed and their statistical characteristics obtained. A relationship for the heating effect with pump parameters was deduced and will be used in developing a model for the energy absorption rate with a theoretical heating model and measurement data in further work.

Acknowledgments We are grateful to Prof. Cesar and Dr. Rietveld for assisting with the experiment. This work was supported by the National Natural Science Foundation of China (Grant nos. 40831062, 41004065), National Supportive Project of Science and Technology of China (Grant no. 2006BAB18B06), the State Key Laboratory of Space Weather (Grant no. 08262DAA4S) and National Key Laboratory of Electromagnetic Environment.

References

1 Rietveld M T, Isham B, Kohl H, et al. Measurements of HF-enhanced plasma and ion lines at EISCAT with high-altitude resolution. Journal of Geophysical Research, 2000, 105(A4): 7429–7439
2 Borisov N D, Hagfors T. Excitation of heater-enhanced plasma and ion lines near the reflection level of a high-frequency pump wave. Journal of Plasma Physics, 2001, 66: 71–89
3 Ashrafi M, Kosch M J, Honary F. Heater-induced altitude descent of EISCAT UHF ion line enhancements: Observations and modeling. Advances in Space Research, 2006, 38(11): 2645–2652
4 Mantas G P. Large 6300-°A airglow intensity enhancements observed in ionosphere heating experiments are exited by thermal electrons. Journal of Geophysical Research, 1994, 99(A5): 8993–9002
5 Gurevich A V, Milikh G M. Artificial airglow due to modifications of the ionosphere by powerful radio waves. Journal of Geophysical Research, 1997, 102(A1): 389–394
6 Barr R. The generation of ELF and VLF radio waves in the ionosphere using powerful HF transmitters. Advances in Space Research, 1998, 21(5): 677–687
7 Djuth F, Stubbe P, Sulzer M P, et al. Altitude characteristics of plasma turbulence excited with the Tromsø superheater. Journal of Geophysical Research, 1994, 99(A1): 333–339
8 Gordon W E, Carlson H C. Ionospheric heating at Arecibo: first tests. J Geophys Res, 1971, 76: 7808–7813
9 Gordon W E, Carlson H C. Arecibo heating experiments. Radio Sci, 1974, 9: 1041–1047
10 Mantas G P, Carlson H C, LaHoz C H. Thermal response of the F region ionosphere in artificial modification experiments by HF radio waves. J Geophys Res, 1981, 86: 561–571
11 Djuth F T, Thide B, Lerkic H M, et al. Large F region electron-temperature enhancements generated by high-power HF radio waves. Geophys Res Lett, 1987, 14: 953–956
12 Jones T B, Robinson T, Kopka H, et al. Phase changes induced in a diagnostic radio wave passing through a heated region of the aurora ionosphere. J Geophys Res, 1982, 87(A3): 1557–1564
13 Jones T B, Robinson T, Stubbe P, et al. EISCAT observation of heated ionosphere. J Atmos Terr Phys, 1986, 48(A1): 1027–1035
14 Stocker A J, Honary F, Robinson T R, et al. EISCAT observation of large scale electron temperature and density perturbations caused by high power HF radio waves. J Atmos Terr Phys, 1992, 54(11/12): 6285–6297
15 Rietveld M T, Kosch M J, Blagoveshchenskaya N F, et al. Ionospheric electron heating, optical emissions and striations induced by powerful HF radio waves at high latitude: aspect angle dependence. J Geophys Res, 2003, 108 (A4): doi 10 1029/2002 JA009543
16 Kero A, Bosinger T, Pollar P, et al. First EISCAT measurement of

electron-gas temperature in the artificially heated D-region ionosphere. Annales Geophysicae, 2000, 18: 1210–1215

17 Xu B, Wu J, Wu Z S, et al. The temperature enhancement induced by ionosphere heating in low region. Progress in natural science, 2008, 18(11):1339–1343

18 Honary F, Stocker A J, Robinson T R, et al. EISCAT observations of electron temperature oscillations due to the action of high power HF radio waves. J Atmos Terr Phys, 1993, 55(10): 1433–1448

19 Saito, S, Buchert, S, Nozawa, S, et al. Observation of isotropic electron temperature in the turbulent E region. Annales Geophysicae, 2001, 19: 11–15

20 Lofas H, Ivchenko N, Gustavsson B, et al. F-region electron heating by X-mode radiowaves in underdense conditions, Annales Geophysicae, 2009, 27: 2585–2592.

21 Huang W G, Gu S F, Gong J C. Ionospheric heating by powerful high-frequency radio waves. Journal of Radio Science, 2004, 19(3): 296–301(in Chinese)

22 Blagoveshchenskaya N F, Carlson H C, Kornienko V A, et al. Phenomena induced by powerful HF pumping towards magnetic zenith with a frequency near the F-region critical frequency and the third electron gyro harmonic frequency, Annales Geophysicae,2009, 27, 131–1